JACS
JOURNAL OF THE AMERICAN CHEMICAL SOCIETY
Article
pubs.acs.org/JACS

Hole Transfer Dynamics from a CdSe/CdS Quantum Rod to a Tethered Ferrocene Derivative

Kartick Tarafder,[†,‡] Yogesh Surendranath,[†,§,∥,⊥] Jacob H. Olshansky,[†,§,∥] A. Paul Alivisatos,[†,§,∥] and Lin-Wang Wang*[,†]

[†]Materials Science Division, Lawrence Berkeley National Laboratory, Berkeley, California 94720, United States
[‡]Department of Physics, BITS-PILANI Hyderabad Campus, Andhra Pradesh 500078, India
[§]Department of Chemistry, University of California, Berkeley, California 94720, United States
[∥]Kavli Energy Nanosciences Institute, University of California, Berkeley, California 94720, United States
[⊥]Miller Institute for Basic Research in Science, University of California, Berkeley, California 94720, United States

Supporting Information

ABSTRACT: Hole transfer between a CdSe/CdS core/shell semiconductor nanorod and a surface-ligated alkyl ferrocene is investigated by a combination of ab initio quantum chemistry calculations and electrochemical and time-resolved photoluminescence measurements. The calculated driving force for hole transfer corresponds well with electrochemical measurements of nanorods partially ligated by 6-ferrocenylhexanethiolate. The calculations and the experiments suggest that single step hole transfer from the valence band to ferrocene is in the Marcus inverted region. Additionally, time-resolved photoluminescence data suggest that two-step hole transfer to ferrocene mediated by a deep trap state is unlikely. However, the calculations also suggest that shallow surface states of the CdS shell could play a significant role in mediating hole transfer as long as their energies are close enough to the nanorod highest occupied molecular orbital energy. Regardless of the detailed mechanism of hole transfer, our results suggest that holes may be extracted more efficiently from well-passivated nanocrystals by reducing the energetic driving force for hole transfer, thus minimizing energetic losses.

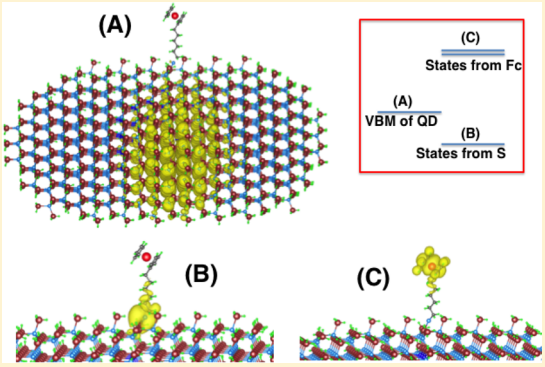

INTRODUCTION

Semiconductor nanocrystals have emerged as attractive candidates for use in next generation optoelectronic devices and photocatalytic energy conversion schemes.[1−6] Owing to their size-tunable bandgaps, high extinction coefficients, and facile wet chemical syntheses, cadmium chalcogenide nanomaterials have shown particular promise for photocatalytic proton reduction and as sensitizers in photovoltaics.[7−9] While photoexcited electrons in these nanomaterials are sufficiently reducing to drive hydrogen evolution in the presence of a catalyst, the residual hole typically drives oxidative photocorrosion, necessitating the use of a sacrificial electron donor in order to sustain photocatalysis. Unfortunately, the use of sacrificial donors limits the utility of the photocatalytic scheme and severely diminishes the energy stored in the net reaction. Moreover, the identity of the sacrificial donor is often the key determinant of the chemical quantum yield for photocatalysis, suggesting that the rate determining process is hole extraction from the nanocrystal rather than electron transfer to a hydrogen evolving catalyst.[7,10] Similarly, in quantum dot (QD) sensitized solar cells the photoexcited electron can be efficiently injected into an n-type metal oxide (e.g., TiO_2), yet again the residual hole drives photocorrosion.[11] To overcome this problem, researchers have used blocking layers[12] and the polysulfide/sulfide redox couple[13,14] to passivate the surface of the QD, yet both these strategies introduce new kinetic barriers to charge transfer.[15] Thus, a detailed understanding of interfacial hole transfer dynamics from semiconductor nanocrystals is a prerequisite for the rational design of more robust and active photocatalysts and sensitizers for photovoltaics.

Interfacial charge transfer processes are well described by Marcus theory,[16,17] which quantitatively describes the dependence of the rate on the driving force, electronic coupling, and inner- and outer-sphere reorganizational energies. In the Marcus normal region, rate increases with driving force. Therefore, improvements in the interfacial charge transfer rate will be tempered by losses in total energy stored in a QD-based photocatalytic or photoelectrochemical scheme. Previous studies have indicated that electron transfer from photoexcited QDs lies in the normal region. For example, by systematic reduction of the QD size, the electron transfer from CdSe QDs to TiO_2 particles was studied, and it was concluded that this transfer is in the normal region of Marcus theory.[18] However,

Received: January 27, 2014
Published: March 10, 2014

   dx.doi.org/10.1021/ja500936n | J. Am. Chem. Soc. 2014, 136, 5121−5131

quantum confinement does not significantly modulate the VB maximum, preventing an analogous study of hole transfer from cadmium chalcogenide QDs. Alternatively, systematic probing of the driving force−rate relationship for hole transfer is also possible through modulation of the redox potential of the electron donor. Although hole transfer from QDs to surface bound molecules has been investigated,[19−25] no clear driving force/rate relationship has been uncovered because of a lack of control over the number of electron donors, or their separation from the QD surface.

In particular, a microscopic understanding of these systems is still lacking and there is no direct comparison between experiment and first principle theory. One of the difficulties comes from theoretical modeling of such systems. Quantitative understanding and comparison with experiment require atomistic ab initio calculations, yet the thousands of atoms in the system prevent the direct deployment of ab initio methods. Although there are many ab initio calculations of charge transfer rates based on Marcus theory for molecular systems,[26] we are aware of no corresponding studies on nanostructured QDs. In a recent article,[27] Knowles et.al. have reviewed the use of Marcus theory to study charge transfer from QDs to surface bound electron and hole accepting molecules. The difficulties of determining the bonding and coupling of the surface molecules to the QD (e.g., the possible different configurations of physisorption), the theoretical difficulty of calculating large QD systems, and the difficulties of experimentally measuring the chemical driving forces were fully discussed. It is thus highly desirable to have a well controlled system where the molecule to QD attachment is well understood (e.g., with a ligand chemical bond) and a high level ab initio calculation of such a system based on Marcus theory, which allows for a direct comparison between theory and experiment. Not only can this verify the validity of Marcus theory, it can also reveal some of the microscopic mechanisms of the charge transfer, e.g., the possible role of surface intermediate states, the relative importance of the electronic coupling constant versus the driving force and reorganization energy, and whether the system is in the normal or inverted Marcus region. Herein we apply a charge patching method[28] to compute charge transfer rates between a CdSe/CdS quantum rod and a surface tethered ferrocene derivative. To overcome the error associated with conventional density functional theory (DFT) in determining the band gap and orbital levels, we apply the many body perturbation GW method. Our theoretical work represents a general approach for studying nanostructure charge transfer processes within the framework of Marcus theory. Furthermore, our silyl transfer ligand exchange technique provides us with confidence about the ligand passivation and anchoring atomic structures.

We use a type II core shell quantum rod as the light absorber because it displays high photostability, enhanced photoluminescence quantum yield, efficient electron−hole separation, and a reduced role of the surface states.[29−32] For the CdSe/CdS core/shell structure it has been found that the electron can be extracted efficiently by a metal tip at one end of a long nanorod, leaving the hole confined to the CdSe core.[33,34] This is because the valence band maximum (VBM) of the core/shell QD is localized within the CdSe core. The current study employs ab initio calculations which suggest that hole transfer from a photoexcited core/shell CdSe/CdS quantum rod to a tethered ferrocene (Fc) moiety is in the inverted region of Marcus theory. Experimental evidence qualitatively matches the theory in both measured driving force and charge transfer rate. This implies that rapid hole transfer rates may be retained with the use of less reducing electron donors, thereby providing an avenue to improve efficiency in QD based energy conversion schemes.

EXPERIMENTAL METHODS

Chemicals. All chemicals were used as received unless stated otherwise: 6-(ferrocenyl)hexanethiol (Fc-hex-SH, Sigma-Aldrich), trimethylsilyl cyanide (TMS-CN, 98%, Sigma-Aldrich), 1-octanethiol (Oct-SH, 98.5+%, Sigma-Aldrich), cadmium oxide (CdO, 99.99%, Sigma-Aldrich), tri-*n*-octylphosphine oxide (TOPO, 99%, Strem), tri-*n*-octylphosphine (TOP, 99%, Strem), octadecylphosphonic acid (ODPA, 99%, PCI Synthesis), hexylphosphonic acid (HPA, 99%, PCI Synthesis), selenium (Se, 99.99%, Sigma-Aldrich), sulfur (S, 99.9995% Alfa Aesar), toluene-d_8 (99.6%, Sigma-Aldrich), tetrabutylammonium hexafluorophosphate (TBA-PF_6, 99.0+%, Fluka), bis(pentamethylcyclopentadienyl)iron(II) (Fc*, 97%, Sigma-Aldrich), ferrocene (Fc, 98%, Sigma-Aldrich), 1,2-ethanedithiol (EDT, 90+%, Sigma-Aldrich), and anhydrous solvents including chloroform, methanol, toluene, acetonitrile, and dichlorobenzene.

CdSe/CdS Quantum Rod Synthesis. Small aspect ratio rods were prepared by modifying a reported procedure.[35] See Supporting Information for synthetic details.

Ligand Synthesis. *Compound 1.* Freshly distilled TMS-CN (2.4 g, 24 mmol) and Fc-hex-SH (250 mg, 0.83 mmol) were loaded into a dried, septum-capped vial equipped with a stir bar. The reaction mixture was heated under argon at 100 °C for 2.5 h and then placed under vacuum at 60 °C for 7 h to remove excess TMS-CN to yield a red oil. ^{1}H NMR (400 MHz, $CDCl_3$) δ 4.25 (s, 5H), 4.20 (m, 4H), 2.49 (t, 2H), 2.32 (t, 2H), 1.7−1.1 (m, 13H), 0.30 (s, 9H)

Compound 2. Freshly distilled TMS-CN (2.46 g, 24.8 mmol) and Oct-SH (1.1 g, 7.5 mmol) were loaded into a dried, septum-capped vial equipped with a stir bar. The reaction mixture was heated under argon at 100 °C for 2.5 h and then placed under vacuum at 60 °C for 7 h to remove excess TMS-CN. The crude product was then vacuum-distilled, with collection starting at 45 °C, 550 mtorr, and discarding of the first few drops: clear oil, 0.86 g, 52% yield. ^{1}H NMR (400 MHz, $CDCl_3$) δ 2.47 (t, 2H), 1.59 (quin, 2H), 1.38 (quin, 2H), 1.27 (m, 10H), 0.87 (t, 3H), 0.31 (s, 9H).

Ligand Exchange of CdSe/CdS Quantum Rods. The absorption peak of the CdSe core was used to determine the concentration of rods in the stock solution by using empirical extinction coefficient calibrations developed for QDs without shells.[36] There is therefore some uncertainty in this value, which we measured to be 130 μM. The ligand exchange reactions were performed in two NMR tubes, each with 250 μL of this stock solution. Compound **1** (80 μL, ∼0.17 mmol) was added to one tube, and compound **2** (50 μL, ∼0.18 mmol) was added to the other tube. Both NMR tubes were sealed under argon and heated to 100 °C for 3 days. Reaction progress was monitored with ^{31}P NMR by observing liberation of silylated ODPA. Both solutions were cleaned in inert atmosphere by precipitation, centrifugation, and resuspension three times with methanol as the nonsolvent and once with acetonitrile as the nonsolvent. The resuspension solvents (in order) were chloroform, dichlorobenzene, toluene, and toluene-d_8. The resultant deuterated toluene solutions were centrifuged to remove insoluble impurities and stored under inert atmosphere.

Optical Spectroscopy. Measurements were performed on dilute solutions of nanoparticles dispersed in toluene or chloroform in 1 cm cuvettes. Absorption spectra were collected on a Shimadzu 3600 spectrophotometer with 1 nm increments and solvent background subtraction. Emission spectra were acquired on a Horiba Jobin Yvon TRIAX 320 Fluorolog. Fluorescence lifetime measurements for Fc-hex-SH exchanged rods were performed in chloroform on a Pico Quant FluoTime 300 with a PMA 175 detector and an LDH-P-C-405 diode laser (excitation wavelength of 407.1 nm). Lifetime measurements on the native and Oct-SH exchanged rods were performed on a Horiba Jobin Yvon Fluorolog spectrofluorometer with a PMT detector

dx.doi.org/10.1021/ja500936n | J. Am. Chem. Soc. 2014, 136, 5121−5131

and a nanoLED 440 nm excitation source. Quantum yields were determined by comparison to a standard sample of rhodamine 6G in absolute ethanol, which has a 95% quantum yield as reported by the vendor (Exciton).

Cyclic Voltammetry: General Methods. All electrochemical measurements were conducted using a CHI-600C electrochemical analyzer and were performed in an argon atmosphere. Unless otherwise stated, a platinum mesh served as the counter electrode and a silver wire served as the pseudo reference electrode and 0.1 M TBA-PF_6 as the supporting electrolyte.

Determination of Fc-hex-SH/Fc-hex-SH$^+$ Potential. Cyclic voltammograms were recorded from quiescent chloroform electrolyte solution using a 3.0 mm diameter glassy carbon button working electrode. The concentration of Fc-hex-SH was approximately 330 μM. CV scans were recorded at 10 mV/s, and the formal reduction potential $E_{1/2}$ was taken at the average of the oxidation and reduction peak potentials. All potentials were calibrated using an Fc* internal standard ($E_{1/2}$ = −483 mV vs Fc/Fc^+ in chloroform)[37] added to the electrochemical cell and are reported versus Fc/Fc^+.

Determination of QD CB Potential. A QD film coated working electrode was prepared by drop casting an ∼150 μM solution of Fc-hex-SH functionalized seeded rods dispersed in toluene onto an indium tin oxide (ITO) coated glass slide. Upon solvent evaporation, the slide was incubated in a 181 mM solution of EDT in methanol at 50 °C for 16 h. This treatment served to cross-link the particles, increasing the adhesion and electrical conductivity of the film. The slide was then washed with chloroform and placed in a solution of 0.1 M TBA-PF_6 in acetonitrile for electrochemical measurements. To minimize oxidative or reductive decomposition of the film upon electrochemical charging, CV scans were recorded at −40 °C and referenced to the Fc/Fc^+ redox couple added after the measurement.

Computational Procedure. We have constructed a CdSe spherical core with a 2.5 nm diameter embedded in a CdS nanorod that is 7.2 nm in length and 3.8 nm in diameter as shown in Figure 1A. While this nanorod has the same diameter as the experimental nanorod (see Figure S1), it is slightly shorter in length. However, since the hole will be localized in the CdSe spherical core and will engage in vectorial charge transfer orthogonal to the long axis of the nanorod, we believe that this discrepancy will not significantly impact the calculated hole transfer rate constant. A Fc functional group is linked with a -$(CH_2)_6$-S- (6-hexanethiolate) chain, to form the conjugated structure shown in Figure 1B. When this ligand is attached to the (101−0) basal plane of the CdSe/CdS nanorod, the thiolate group -S is ligated to a single Cd surface atom as shown in Figure 1(C). The atomic structure of the linkage is shown in Figure 1D. To simplify the computation, we have only decorated the quantum rod with a single surface tethered ferrocene electron donor. The effects of multiple ligands will be included later. Although there could be some uncertainties for the actual anchoring configuration, the experimentally demonstrated strong ligand binding indicates that there is a covalent bond between the Fc-hex-S- molecule and the QD (see the Experimental Methods for the ligand exchange method). Thus, it makes most chemical sense to bond one Fc-hex-S- molecule to one Cd atom on the surface. To reduce the possible effects of surface dipoles[38] and surface states, we have chosen to terminate all other surface exposed atoms with pseudo-hydrogen atoms. Such artificial surface passivation will push surface trap states out of the band gap. We will investigate the possible role of surface states later with both experimental and theoretical methods. Overall there are 3453 atoms in the system. This is significantly larger than systems amenable to performing direct DFT calculations. Therefore, we employ a multilevel divide-and-conquer strategy. First, the charge density of the core/shell QD system (Figure 1A) is generated with the charge patching method (CPM).[39] It has been shown that for systems without long-range electric fields (e.g., no overall dipole moment, as in the system studied), the CPM can yield essentially the same QD charge density as in a self-consistent DFT calculation. The resulting orbital eigen energy error is only about 20 meV. To construct the total charge density of the Fc-hex-S attached to the rod, we cut out part of the QD with the molecule attached to it into a separated subsystem as indicated by Figure 1E. The cutoff bonds are passivated with pseudo-hydrogen atoms. This subsystem with 588 total atoms can be calculated with a direct DFT method. The atomic positions of the molecule and the atoms near the anchoring sites are fully relaxed using our plane wave nonlocal pseudo-potential DFT code PEtot.[40] Finally, the total charge density of the Fc-hex-S linked to the QD is constructed by patching the charge density of the QD (Figure 1A) constructed from the CPM with the charge density of the subsystem (Figure 1E), with a region of gradation shown as the dashed line in Figure 1C. This is the same procedure that has been used in a previous connected QD calculation.[41] The electrostatic potential V_{es} for the whole system is then obtained from the total patched charge density $\rho(r)$ by solving Poisson's equation. With this V_{es} (which also includes the nuclear pseudo-potential contributions), the DFT single particle equation is given by

$$H\psi_i = \left\{-\frac{1}{2}\nabla^2 + V_{es} + V_{xc} + \hat{V}_{NL}\right\}\psi_i = \varepsilon_i\psi_i \quad (1)$$

where $V_{xc}(\rho(r))$ is the LDA exchange correlation potential and $\hat{V}_{NL}$ is the nonlocal part of the atomic pseudo-potentials implemented with the Kleinman−Bylander form.[42] On the basis of this single particle Hamiltonian, we used the generalized moment method (GMM)[43] to calculate the total and local density of states (DOS) and used the folded spectrum method (FSM)[44] to determine eigenstates and eigenenergies near the band edge region. The FSM uses a conjugate-gradient iteration technique to solve $(H - \varepsilon_{ref})^2\psi_i = (\varepsilon_i - \varepsilon_{ref})^2\psi_i$ instead of using eq 1 directly. Here ε_{ref} is a reference energy placed inside the band gap. We calculate the hole transfer rate from the QD to Fc based on Marcus theory by first calculating the quasi-particle energy as defined in the GW equation. As it is impossible to calculate the GW equation directly for such a large system, we introduce several corrections to the DFT Kohn−Sham eq 1. We will also include reorganization energies in order to convert the quasi-particle eigenenergies into the total charging energies (which include the atomic relaxation parts) used in Marcus theory.

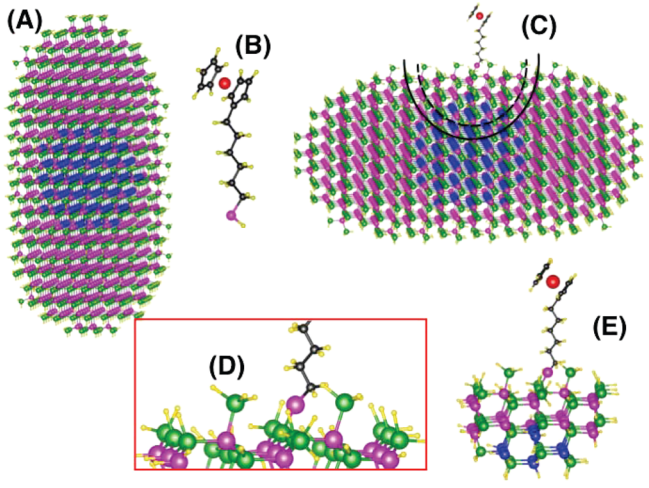

Figure 1. Computational scheme for obtaining the total charge density of a ferrocene attached CdSe/CdS core/shell nano rod. (A) Core/shell structure of the nano rod where CdSe core (blue) is embedded inside CdS rod (purple). (B) Geometric structure of an isolated Fc-hex-SH. (C) Geometric structure of a Fc-hex-S ligand attached to the rod. The detailed atomic structure of the linkage is in the inset (D). (E) Small portion of QD with the Fc-hex-S- ligand cut out from Fc-hex-S-QD, indicated as a black solid line in part C. Charge density of this subsystem will be generated directly from the DFT calculation. The total charge density will be generated using this charge density together with the patched charge density of the rod in part A through a smooth cutoff indicated as a black dashed line in part C.

dx.doi.org/10.1021/ja500936n | J. Am. Chem. Soc. 2014, 136, 5121−5131

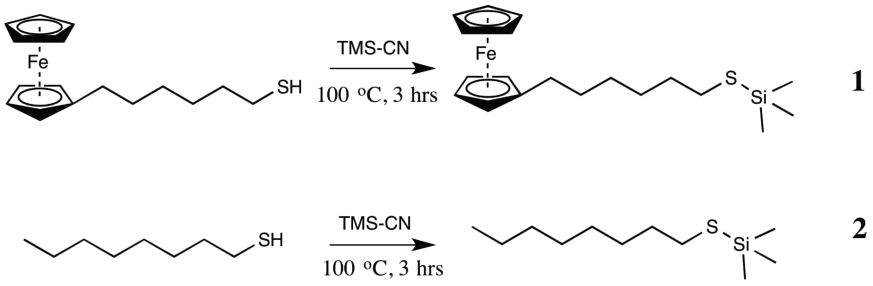

Figure 2. Synthetic scheme for the preparation of ligand precursors **1** and **2** by protection of the thiol binding head with a trimethylsilyl group.

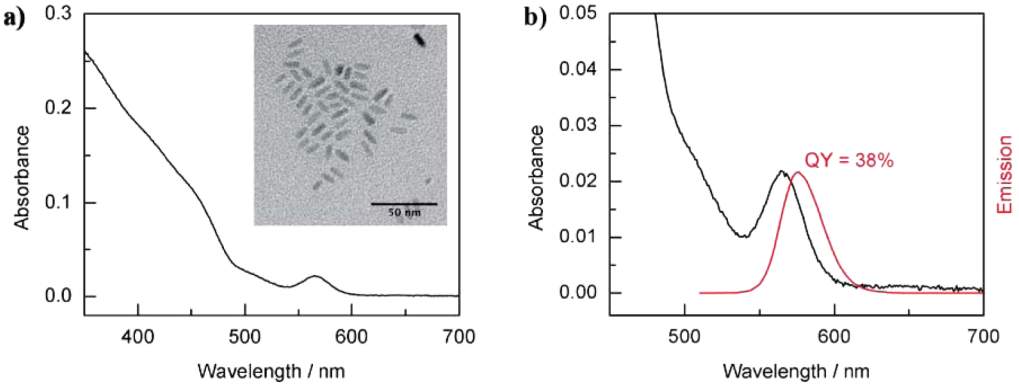

Figure 3. Characterization of the as-synthesized CdSe/CdS nanorods: (a) absorption spectrum of the rods in toluene with TEM micrograph inset; (b) absorption and emission spectra overlay with emission intensity scaled to core absorption maximum.

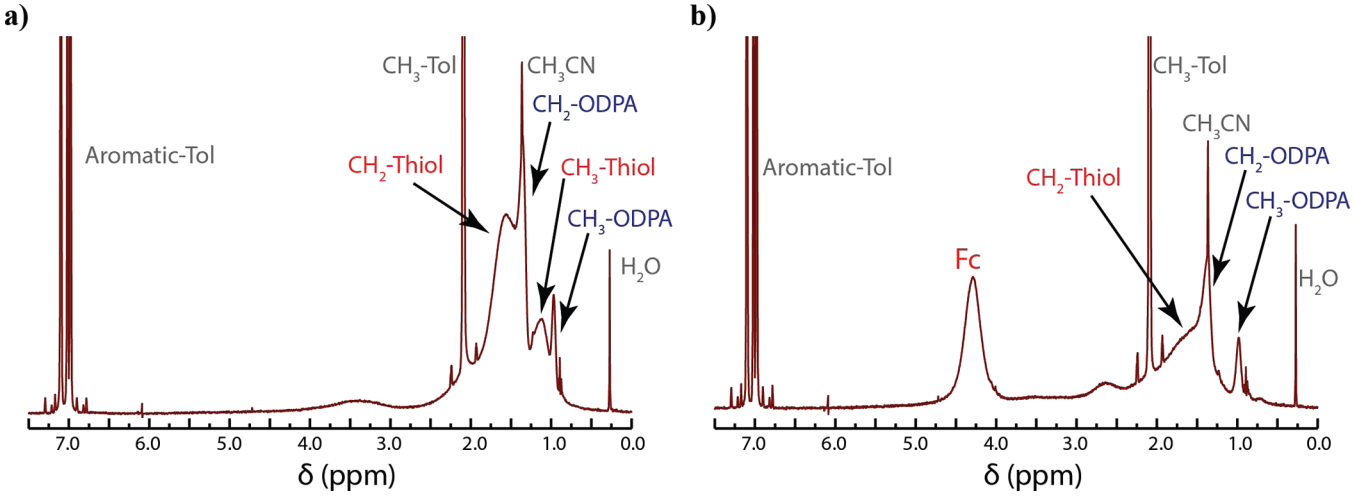

Figure 4. ^{1}H NMR spectra of (a) Oct-S exchanged and (b) Fc-hex-S exchanged rods.

RESULTS AND DISCUSSION

Experimental System. CdSe/CdS nanorods were synthesized with dimensions of 11.3 ± 1.5 nm by 4.4 ± 0.5 nm with N = 100 rods measured (see Supporting Information for sizing distribution). Figure 3a shows the TEM image and optical absorption spectrum of the CdSe/CdS nanorods. Figure 3b shows that the photoluminescence (PL) peak overlaps with the first optical absorption peak, thus indicating that emission is from an excited state in which the hole is localized inside the CdSe core. The PL quantum yield is 38%, indicating suppression of trap state mediated nonradiative decay such that the radiative and nonradiative rates are commensurate. The emission maximum lies at 564 nm, corresponding to a band gap in the CdSe core of 2.2 eV.

Silyl transfer ligand exchange was performed on the as-synthesized seeded rods to drive the removal of the strongly bound native phosphonate ligands. This method has been used previously to strip phosphonate ligands off QD surfaces.[45,46] Ligand precursors were prepared by exchanging trimethylsilyl (TMS) groups for the thiol proton on both Fc-hex-SH and Oct-SH (yielding compounds **1** and **2**). The scheme is illustrated in Figure 2. During ligand exchange, the TMS group transfers to and liberates the phosphonate ligand, leaving the thiolate ligand bound to the surface Cd atoms. Oct-SH was used as a control, since the nature of the ligand binding group has been shown to influence PL quantum yield and luminescence lifetime.[47] Therefore, we could compare thiol capped seeded rods with and without the Fc hole acceptor. Figure 4 shows the ^{1}H NMR spectra of the Oct-S- and Fc-hex-

dx.doi.org/10.1021/ja500936n | J. Am. Chem. Soc. 2014, 136, 5121−5131

S- exchanged rods (Figure 4a and Figure 4b, respectively). One sees the strong peak at ~4.3 ppm corresponding to bound Fc aromatic protons after ligand exchange in Figure 4b. The broadness of this peak indicates that all Fc-hex-S molecules are bound to the QD surface. Broadening of NMR peaks associated with ligands bound to QDs has been observed before and is attributed to fast transverse (or spin−spin) relaxation owing to the slow tumbling time of QDs in solution.[48] Judged by the integrated area of the Fc aromatic proton peak compared to the CH_3 peak from residual ODPA, one can conclude that the majority of the surface ligand has been exchanged to Fc-hex-S.

LDA Density of States. Figure 5A shows the density of states (DOS) of the quantum rod−alkyl ferrocene conjugate.

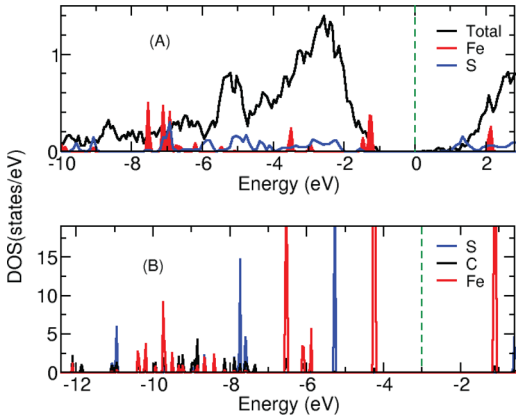

Figure 5. Total (black) and Fe (red) and S (blue) atom projected density of states of the whole system (system C shown in Figure 1) with Fc attached to the QD (A). Fe (red), S (blue), and C (black) atom projected density of states of an isolated Fc-hex-SH molecule (system B shown in Figure 1).

The black curve represents the total DOS. The red and blue curves are projected density of states (PDOS) at the Fe atom and the anchoring S atom, respectively. We have compared these PDOS with the PDOS of the isolated Fc-hex-SH molecule shown in Figure 5B. After an energy shift to align them together, we can see that the PDOS on the Fe atom is almost the same for these two systems. However, the sharp peaks of the S PDOS in the separated molecule have been broadened significantly in the attached case, and in some regions the energies have been shifted significantly (e.g., in the conduction band). This is expected, since the S atom has a significantly altered bonding environment in the attached case. In agreement with experimental observation,[49] our Fe PDOS shows a doubly degenerate HOMO state at −4.26 eV, consisting of two pure 3d states.

The HOMO and LUMO states of the Fc molecule are both located at the Fe atom, as occupied and unoccupied d orbitals, respectively. The LDA HOMO−LUMO gap of the Fc is 3.18 eV, which is much smaller than the experimental value (~6.0 eV),[50,49] as expected because of the LDA band gap error. The LDA result should describe accurately the possible dipole moment between the QD and the molecule, and their relative electrostatic potentials. Thus, it provides a baseline to obtain the more accurate orbital level alignments between the QD and molecule as described below.

The LDA orbital level alignment as derived from the density of states is depicted in Figure 6 under the LDA label. Using the FSM, we also obtained explicitly the HOMO level in the QD, as shown in Figure 7A, and the HOMO level in the Fc, as shown in Figure 7C. We notice a state located at the S atom anchoring the QD as depicted in Figure 7B. This state in Figure 7B has a lower energy than the HOMO of the QD as shown in the inset of Figure 7. Nevertheless, it provides another possible channel for charge transfer, as will be discussed later.

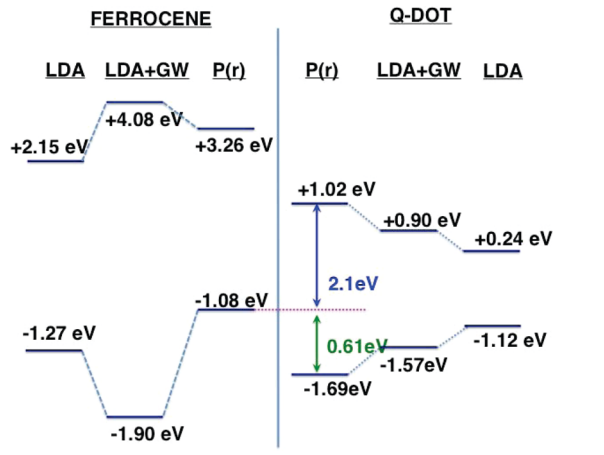

Figure 6. Correction of quasi particle energy ϵ_{QD}, ϵ_{MOL} using GW and polarization corrections. $P(r)$ indicates the levels after the GW, and $P(r)$ effects are added on top of the LDA results.

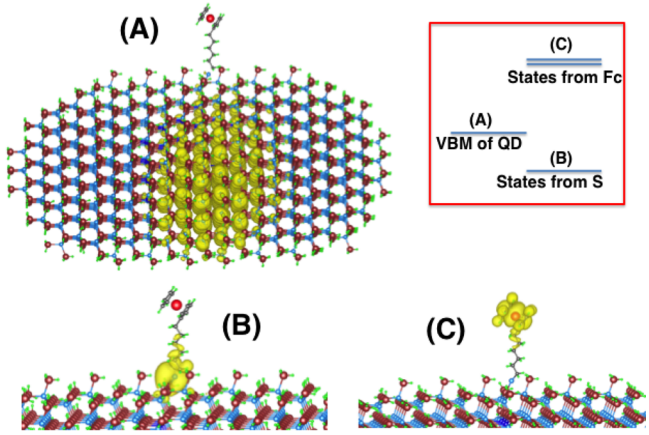

Figure 7. Wave function isosurface plots for QD HOMO state (A), the state at the S- anchoring site (B), and the ferrocene HOMO state (C). Their relative energies are shown in the inset.

GW Corrections. In order to apply Marcus theory, we must calculate the energy difference between the system when the hole resides within the QD and after hole transfer to Fc. These reactant and product state energies include electronic and atomic relaxation components. The electronic components are related to the $E(N)-E(N-1)$ energies for the QD HOMO state and Fc molecule HOMO state. Here $E(N)$ and $E(N-1)$ are the total energies of the system with N and $N-1$ electrons (but with the same atomic positions in the $E(N)$ and $E(N-1)$ systems). By definition, the $E(N)-E(N-1)$ energies are the quasi-particle energies for the QD HOMO state (or Fc HOMO state) as described in the many-body GW equation.[51] In practice, it is impossible to calculate the GW quasi-particle energies directly for a thousand-atom system. We thus calculate these energies by additional corrections on top of the LDA Kohn−Sham eigenenergies. In the G0W0 calculation[52] the LDA local exchange correlation potential V_{xc} in eq 1 is replaced

dx.doi.org/10.1021/ja500936n | J. Am. Chem. Soc. 2014, 136, 5121−5131

by a nonlocal self-energy term $\Sigma(r,r')$. There are two correction terms when V_{xc} is replaced by $\Sigma(r,r')$.[53] The first correction term is a short-range term, which decays exponentially as a function of $|r - r'|$ over one bond distance for a given r, and it can be obtained from a bulk (e.g., bulk CdSe) or isolated molecule (for Fc) calculation. The second is a long-range term, which manifests itself as a polarization energy and will be discussed in the next section. Using a bulk G0W0 calculation (with the LDA electrostatic potential V_{es}), one can obtain the absolute LDA to GW energy shifts for the HOMO and LUMO levels separately. The same is true for the Fc molecule (here, only the Fc molecule without the hex-SH tail is used). The GW corrected orbital alignment is shown as LDA + GW in Figure 6. Note that for the Fc levels, the occupied states are shifted downward by 0.6 eV while the unoccupied states are shifted upward by 1.9 eV. Now the corrected quasi-particle HOMO−LUMO gap is 5.6 eV, which is close to the experimental electron affinity and ionization energy gap of ∼6 eV for ferrocene in the gas phase.[49] For bulk CdSe, the conduction band minimum (CBM, which is also the LUMO) and valence band maximum (VBM, which is also the HOMO) corrections are 0.66 and −0.45 eV, respectively, leading to a 1.8 eV bulk energy band gap, in agreement with experiment.

Polarization Correction. In nanosystems, the GW self-energy Σ has a long-range term due to the long-range behavior of the dielectric function. It has been shown that the dynamic screening effects of this long-range term can be ignored.[54,55] Under the static Coulomb hole screened exchange (COHSEX) GW approximation, this long-range term can be represented as a classical polarization correction.[53] To obtain an accurate energy alignment between the molecule and QD, it is necessary to include this polarization correction. With the polarization potential $P(r)$, the quasi-particle eq 1 becomes

$$H\psi_i = \left\{-\frac{1}{2}\nabla^2 + V_{tot} + \hat{V}_{NL} \pm P(r)\right\}\psi_i = \varepsilon_i\psi_i \tag{2}$$

Here "+" and "−" signs are used for the electron and hole states, respectively, and $V_{tot} = V_{es} + V_{xc}$. The result of eq 2 compared to that of eq 1 will give us the polarization effects, and we will add this polarization effect on top of the short-range GW correction results as described above. Starting with the many-body quasi-particle GW equation, $P(r)$ can be expressed as[53]

$$P(r) = \frac{1}{2}\lim_{r'\to r}[W(r',r) - W_{bulk}(r',r)] \tag{3}$$

where $W(r',r)$ is the screened electrostatic potential of the nanosystem at r' given an external point charge at r. $W_{bulk}(r',r)$ is the analogous quantity for an extended bulk system with the same material everywhere as that at r. To calculate $P(r)$ numerically, we first obtain the electrostatic potential $\phi(r)$ caused by a sharp (δ-like) charge density $\rho_0(r)$ around r_1 under an inhomogeneous dielectric medium $\epsilon(r)$ from Poisson's equation $\nabla \cdot [\epsilon(r)\nabla\phi(r)] = 4\pi\rho_0(r)$. Then $W(r_2,r_1) = \phi(r_2)$. $P(r)$ at multiple points r is calculated in this way, and it is then spline-interpolated to yield the function in the whole spatial region. Eq 2 is then solved using FSM. The final energy levels after including GW effects and polarization effects are plotted in Figure 6 under the label $P(r)$. After all these corrections, the HOMO of Fc (Figure 7C) appears 0.61 eV above the HOMO level of the QD (Figure 7A). The Figure 7B state from the bonded S atom appears at 0.39 eV below the HOMO of the QD.

Marcus Theory. At this point, we are ready to use Marcus theory to calculate the charge transfer rate from the hole in the HOMO of the QD to the HOMO in the tethered Fc molecule. The charge transfer rate in Marcus theory is expressed as

$$\tau^{-1} = |V_c|^2\sqrt{\frac{\pi}{\lambda k_B T\hbar^2}}\exp[-(\lambda + E_f - E_i)^2/(4\lambda k_B T)] \tag{4}$$

where k_B is the Boltzmann constant, T is temperature, V_c is the electronic coupling between the QD HOMO and Fc HOMO states, and λ is the total reorganization energy of the system. E_i and E_f represent the total energy of the system before (initial) and after (final) the charge transfer as shown in Figure 8. First

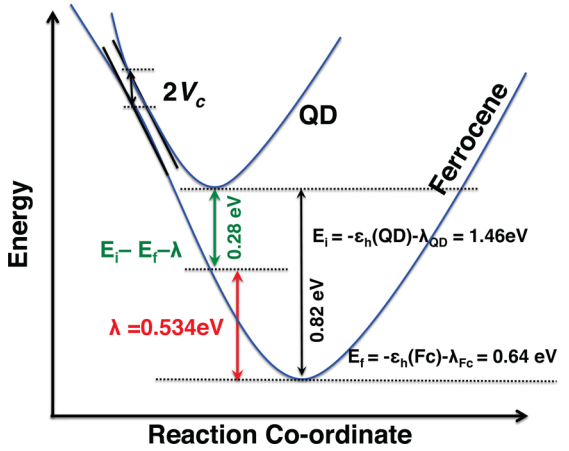

Figure 8. Marcus theory energy diagram. The QD indicates the total energy curve when the hole is located inside the QD, while the ferrocene indicates the total energy curve when the hole is located at the ferrocene.

we must relate the quasi-particle energy levels to E_i and E_f. The initial system is the system with one hole at the HOMO level of the QD (i.e, the $N - 1$ electron system). Thus, its energy $E(N-1)$ should equal the neutral system energy $E(N)$ minus the quasiparticle energy $\epsilon_h(QD)$ by the definition of the quasi-particle energy. However, this is under the assumption that the atomic positions in the neutral (N) and charged ($N - 1$) systems are exactly the same. In reality, after the system is charged ($N - 1$), there is an atomic relaxation energy (reorganization energy) λ_{QD} that will lower the energy of $E(N-1)$ by λ_{QD}. The same is true for the final state after charge transfer, only that the corresponding quasiparticle energy is for the HOMO of the Fc, and the reorganization energy λ_{Fc} is for the charged Fc. Thus, we have

$$E_i = E(N) - [\epsilon_h(QD) + \lambda_{QD}]$$
$$E_f = E(N) - [\epsilon_h(Fc) + \lambda_{Fc}] \tag{5}$$

Note that the common energy $E(N)$ is not important, since only the difference between E_i and E_f will be used in the Marcus equation (eq 4).

Reorganization Energy. The reorganization energies λ_X (X = QD or Fc) include two parts, one for the intrasystem atomic relaxation due to the occupation of the hole state and another for the reorientation of the solvent molecules surrounding the system due to electrostatic screening. We denote them as

dx.doi.org/10.1021/ja500936n | J. Am. Chem. Soc. 2014, 136, 5121−5131

$$\lambda_X = \lambda_X^{at} + \lambda_X^{sol} \quad (6)$$

The λ_{Fc}^{at} can be directly calculated using LDA. One takes the neutral Fc-hex-SH molecule Fc atomic positions and then removes one electron and calculates the electronic self-consistent energy E_0. Then under LDA, one can relax the atomic positions for the +1 charged molecular system and get the ground state energy E_g. Then $\lambda_{Fc}^{at} = E_0 - E_g$. It is found that λ_{Fc}^{at} equals 48 meV as listed in Table 1. One reason for this small value is the relative rigidity of the C_5H_5 rings in the Fc molecule as well as the lack of a dipole moment in the C_6H_{12} chain which could otherwise cause torsional rotation and thus a larger reorganization energy.

Table 1. Reorganization Energies (in meV) of the QD and Ferrocene Molecule from Different Contributions When the QD Is Tethered to a Fc-hex-SH Molecule and Immersed in Chloroform

system	λ_{cc}^{at}	λ_{cc}^{sol}	λ_{CT}^{sol}
ferrocene	48	390	348
QD	138	93	

Theoretically, the λ_{QD}^{at} can be calculated in the same way. However, the large number of atoms in the QD makes such a calculation impractical. In a previous study,[41] we have calculated the atomic reorganization energy of a QD using the electron−phonon coupling constants and phonon modes. It was found that mostly a few acoustic phonon modes are responsible for the atomic relaxation.[41]

The atomic relaxation energy due to the charging of a CdSe QD was tabulated as a function of the QD size, and it is found to be inversely proportional to the QD volume. In the current study, we will use that result. However, in order to convert the previous result (which is for a spherical CdSe QD) to the current system (which is a core/shell nanorod), we calculated the effective volume of the current system HOMO wave function $\psi_h(r)$ as $I = 1/\int|\psi_h(r)|^4\, d^3r$ and compared that to the corresponding spherical CdSe QD value. Since the relaxation energy is caused by the HOMO state and is inversely proportional to its effective volume I, we can use this I and the spherical QD result to estimate the λ_{QD}^{at} for our system. We found our λ_{QD}^{at} to be about 138 meV as listed in Table 1.

Direct calculation of the solvent reorganization energy λ_X^{sol} would be very complex, as it would involve the reorientation of the solvent molecules surrounding X (QD, Fc) in a thermodynamic average.[56] We have thus resorted to the widely used analytical solvent model, where the solvent reorganization energy is expressed as[61]

$$\lambda_X^{sol} = \frac{1}{2}\left(\frac{1}{\epsilon_{op}} - \frac{1}{\epsilon_{st}}\right)\frac{1}{R_X} \quad (7)$$

where R_X is the effective radius of the system and ϵ_{op} and ϵ_{st} are the optical and static dielectric constants, respectively (their difference represents the ionic contribution to the dielectric screening). In the experiment, chloroform is used as the solvent. It has $\epsilon_{op} = 2.08$ and $\epsilon_{st} = 4.81$. When we use the cross-sectional radius of the core/shell nanorod as R_{QD}, the λ_{QD}^{sol} is about 93 meV. This may slightly overestimate the solvent reorganization energy because eq 7 is for a spherical dot, not a long rod. However the error is likely to be only about 10−20 meV. There will also be some error associated with choosing the effective radius for the redox center of the Fc-hex-SH molecule. In the literature, a radius of 4 Å is often used for ferrocene as constructed from the van der Waals radii of the atoms at the periphery.[57,58] This radius seems to yield a reorganization energy close to the experimental values for ferrocene in aqueous solution.[59] However, the effective radius should also depend on the size of the solvent molecules.[60] For the purpose of calculating the dielectric screening induced reorganization energy, it is plausible to assume that the overall effective radius should be the sum of the radius of the charging molecule and the radius of the solvent molecule. Using the solvent densities and an equivalent spherical ball model, one can estimate that the radius of a water molecule is about 1.55 Å, while the radius of a chloroform molecule is 2.55 Å. Thus, we have taken 5 Å as the effective radius of a ferrocene molecule in chloroform, 1 Å larger than its value in water. By use of this radius, the calculated value for λ_{Fc}^{sol} is 390 meV as listed in Table 1.

In eq 4, λ is the reorganization energy after the hole has transferred from the QD to the Fc. The atomic part of this reorganization energy is just a sum of λ_{QD}^{at} and λ_{Fc}^{at}, as both the QD and Fc will relax after the charge transfer. The solvent part, however, is not simply a sum of λ_{QD}^{sol} and λ_{Fc}^{sol}. Because of the short distance between the QD and Fc, some of the solvent molecules originally screening the QD do not need to be completely reoriented to screen the Fc after the charge transfer. As a result, the charge transfer reorganization energy λ_{CT}^{sol} is smaller than $\lambda_{QD}^{sol} + \lambda_{Fc}^{sol}$. More specifically, we have the formula[61]

$$\lambda_{CT}^{sol} = \frac{1}{2}\left(\frac{1}{\epsilon_{op}} - \frac{1}{\epsilon_{st}}\right)\left[\frac{1}{R_{QD}} + \frac{1}{R_{Fc}} - \frac{2}{D}\right] \quad (8)$$

where D is the distance between the center of the QD and the center of the Fc. Thus, we have

$$\lambda = \lambda_{QD}^{at} + \lambda_{MOL}^{at} + \lambda_{CT}^{sol} \quad (9)$$

The calculated λ_{CT}^{sol} is 348 meV; hence, the total λ is 534 meV.

Now if we use the expressions for the reorganization energy from different contributions, we can rewrite the numerator in the exponential part of the Marcus equation (eq 4) as

$$\lambda + E_f - E_i = 2\lambda_{QD}^{at} + \left(\frac{1}{\epsilon_{op}} - \frac{1}{\epsilon_{st}}\right)\left[\frac{1}{R_{QD}} - \frac{1}{D}\right] + \epsilon_h(QD) - \epsilon_h(MOL) \quad (10)$$

Marcus Diagram. Having obtained all the reorganization energies and quasi-particle energies, we can now construct the Marcus energy diagram, as shown in Figure 8. We see that the E_i, E_f difference is 0.82 eV. Since this driving force is calculated to be greater than the total reorganization energy, this suggests that the QD to Fc hole transfer is in the inverted region of Marcus theory. In other words, the value of eq 10 is negative. This means that if we were to raise the E_f energy (e.g., by lowering the Fc HOMO level), not only could we enhance the charge transfer rate, we could also reduce the energy lost in such a transition.

Experimentally, the energy alignment between the QD and the Fc molecule is measured by cyclic voltammetry (CV) as discussed before and shown in Figure 9. The reduction potential of the Fc-hex-SH ligand was determined in chloroform by referencing to the decamethylferrocene (Fc*) redox couple. Using the reported voltage difference between Fc* and

dx.doi.org/10.1021/ja500936n | J. Am. Chem. Soc. 2014, 136, 5121−5131

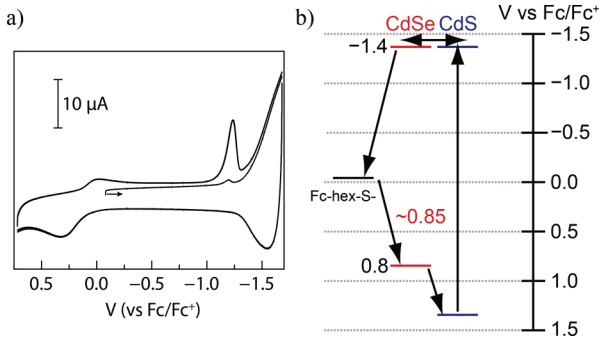

Figure 9. (a) Low temperature CV with a 200 mV s^{-1} scan rate of CdSe/CdS nanorods functionalized with Fc-hex-S and annealed into a film. (b) Energy diagram for various components of the CdSe/CdS nanorod and Fc-hex-S system as determined by cyclic voltammetry and emission data.

Fc,[37] we found that the Fc-hex-SH reduction potential is approximately 50 mV negative of Fc. This 50 mV shift is a result of the mild electron donating nature of the appended alkyl chain on the Fc-hex-SH ligand relative to Fc. The conduction band energy of the CdSe/CdS nanorod was measured by low temperature CV on a thin film of particles. The rods were cross-linked with ethanedithiol to improve conductivity and structural stability of the film. Scans were run reductively to first fill the conduction band (as observed at approximately −1.4 V vs Fc/Fc^+). Removal of conduction band electrons upon scan reversal gives rise to an oxidative feature at −1.4 V as well. The valence band energy level could not be determined directly owing to the limited solvent stability window of acetonitrile. Another feature of this CV is an irreversible reduction peak at −1.2 V. We have not been able to ascribe this peak to a known reduction event but hypothesize that it is a result of irreversible reduction of disulfides within the film to thiolates. Finally, to determine the valence band energy of the CdSe core, we used the fluorescence emission energy of 2.2 eV as the CdSe band gap (see Figure 3). Since the CV measurement is a thermodynamics measurement, it includes all the energy terms (e.g., the reorganization energies) related to the charging of the Fc ligand or the QD. Thus, these energies should be assigned to the E_i and E_f energies in the Marcus diagram of Figure 8. We see that this $E_i - E_f = 0.85$ eV result is rather close to the theoretical 0.82 eV value obtained above. Note that the experimental measurement alone cannot determine whether the charge transfer process is in the normal or inverted region of the Marcus theory. This is determined by the sign of $\lambda + E_f - E_i$. In the future, we plan to verify the hypothesis that this system is in the inverted region experimentally by substitutionally modifying the ligand energy level, although this is beyond the scope of the current work.

Charge Transfer Rate. To use the Marcus formula eq 4 to calculate the charge transfer rate, we also need to calculate the electronic coupling constant V_c between the QD HOMO state $\psi_h(QD)$ and the Fc HOMO state $\psi_h(Fc)$. By definition, $V_c = \langle\psi_h(QD)|\hat{H}|\psi_h(Fc)\rangle$. Here the $\psi_h(QD)$ ($\psi_h(Fc)$) should be the pure QD (Fc) states without the Fc (QD) component. This coupling constant can be calculated by an energy anticrossing between $\epsilon_h(QD)$ and $\epsilon_h(Fc)$ when they are driven by some external potential (e.g., due to reorganization energy fluctuation as in Marcus theory). Computationally, we have added a Gaussian local potential around the Fc molecule to represent such an external fluctuation. This external potential will not change the shape of $\psi_h(Fc)$, but it will drive its energy $\epsilon_h(Fc)$ bypassing the $\epsilon_h(QD)$ energy. At the crossing point, because of their coupling, the two energy curves will anticross each other, and the anticrossing gap is $2V_c$. This is shown in Figure 10.

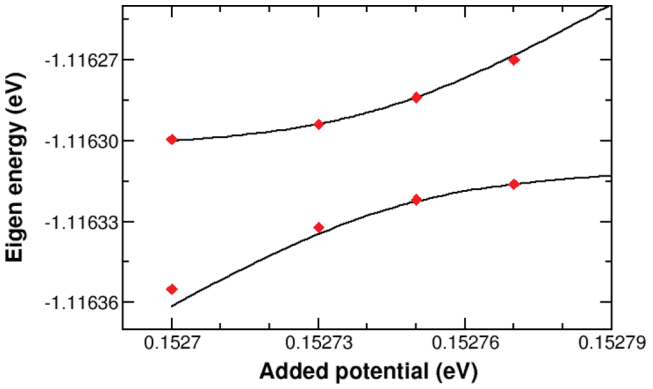

Figure 10. Coupling of the VBM of the QD with Fe-d (Fc-HOMO) state. Red dots indicate the calculated values, and black lines are fitted curves.

Through such calculations, we found that the V_c between the HOMO of the QD (Figure 7A) state and the HOMO of Fc (Figure 7C) is 0.04 meV. This is rather small, owing to the localized nature of the states involved.

Using the above calculated values, we can finally calculate the charge transfer rate from the QD to Fc. The result is 0.86×10^{-5} (1/ps). This rate is small not because of the exponential factor in eq 4, which only amounts to 10^{-1}, but because of the small V_c value. Experimentally, the charge transfer rate is measured by a time-resolved transient PL experiment as shown in Figure 11. It is clear that both the native and Oct-SH

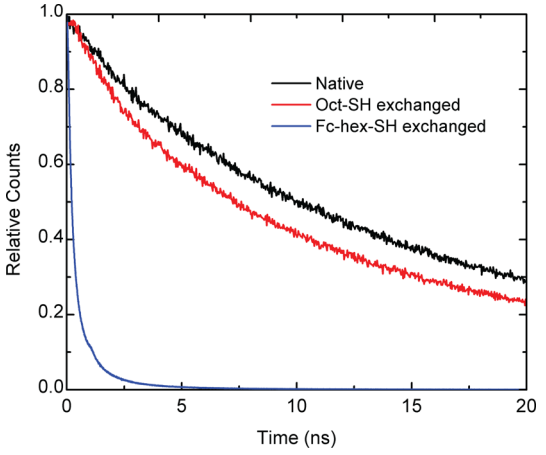

Figure 11. Luminescence lifetime traces of (black) native CdSe/CdS seeded rods, (red) Oct-SH exchanged rods, and (blue) Fc-hex-SH exchanged rods in chloroform.

exchanged rods have much longer lifetimes than the Fc-hex-SH exchanged rods because of rapid nonradiative hole transfer to the Fc, which quenches the radiative emission. The native and Oct-SH exchanged traces were fit to biexponential decays with intensity weighted average lifetimes of 21.0 and 17.0 ns, respectively. Ligand exchange to Oct-SH decreases the lifetime to a small degree, likely because of an increase in surface trap states. These trap states could be a result of thiol capping or

dx.doi.org/10.1021/ja500936n | J. Am. Chem. Soc. 2014, 136, 5121−5131

ligand stripping from the cleaning process. In either case, it does not significantly alter the rate; thus, the rate observed for the Fc-hex-SH exchanged sample can be attributed to hole transfer to Fc. This decay was fit to a triexponential function with time constants of 141 ps, 610 ps, and 2.4 ns. The intensity weighted average lifetime is 790 ps, and the intensity weighted average lifetime of the two shorter decay times is 384 ps (see Supporting Information for fitting details and errors). It is difficult to assign these three decay times to distinct processes because there exists a distribution of rates owing to the range of rod sizes and variation in Fc-hex-S coverage. Therefore, the most we can conclude is that hole transfer for a given nanorod occurs on the time scale of hundreds of picoseconds. Additionally, the hump observed in the fast Fc-hex-S decay is a result of the instrument response function and was accounted for in the exponential fits. See Supporting Information for more details.

In order to compare the experimentally measured PL decay time with our calculated results, we need to take into account the multiple Fc-hex-S molecules bound to the surface of the nanorod. From the experimental ^{1}H NMR measurement shown in Figure 4, we know that there is almost a complete replacement of the surface ligands by Fc-hex-S. Thus, if we assume that each surface Cd atom on the nanorod (101−0) side surface has one Fc-hex-S ligand and if we take only the length of the core diameter in the *c*-axis direction as the effective region for charge transfer, we estimate that there are about 300 Fc-hex-S molecules available for charge transfer on a 3.8 nm diameter nanorod (Figure 12). If we assume all these

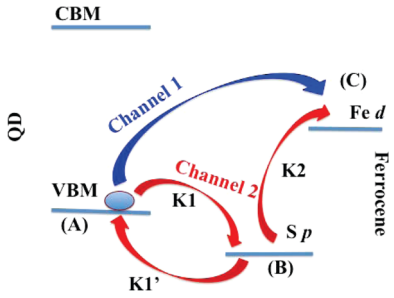

Figure 12. The second possible charge transfer channel with the hole reaches equilibrium between states A and B, then transfers to C from B.

Fc-hex-S molecules have the same charge transfer efficiency, then we have a total charge transfer rate of 2.6×10^{-3} (1/ps), which corresponds to a 388 ps carrier lifetime, well within the range of experimental lifetimes. We would like to add a few points regarding the comparison between theory and experiment in the charge transfer rate. Our calculated nanorod has a diameter of 3.8 nm, although within the distribution of the experimental nanorod widths (Figure S1), it is slightly smaller than the average width of 4.4 nm. If a larger diameter were used, the electronic coupling constant V_c would become smaller, but the number of Fc-hex-S molecules would also increase. We believe that the effect on the lifetime would be rather small. Another effect we have ignored in our theoretical calculation is the existence of the lone electron during the hole transfer. Because of electron−hole Coulomb interaction, there will be an energy cost to separate the hole from the electron when it transfers from the QD to Fc (an increase in the E_f position in Figure 8). However, in a CdSe/CdS core/shell nanorod, the electron is delocalized along the length of the CdS rod.[62] As a result, the electron−hole Coulomb interaction energy would be smaller than 0.1 eV, estimated based on the dimension and dielectric constant. This will not change the qualitative picture and should only affect the lifetime by a factor of 2 according to eq 4 (it would decrease the lifetime).

A Possible Intermediate State Channel. Above, we have calculated the rate for a direct transfer of the hole from the QD HOMO to the Fc HOMO. However, hole transfer may also occur via a localized intermediate state. Specifically, the hole could transfer from the QD HOMO to a surface trap state prior to transferring to the Fc moiety. Surface traps often play prominent roles in the charge dynamics of QDs with effects observed in QD blinking,[63] carrier mobilities in QD solids used for photovoltaics[64] and in explaining the multiexponential PL decays observed in QDs.[65] It is therefore important to consider their role in possibly mediating charge transfer.

This mediated charge transfer can occur via two types of traps: deep traps and shallow traps. A deep trap state will lie within the band gap of the QD and will cause irreversible charge trapping. This can only lead to nonradiative recombination and would therefore be reflected in the PL decays. The experimental decays in Figure 11 indicate that this type of trapping is not involved in hole transfer to Fc. The decay curves for both the native and Oct-SH exchanged rods show that irreversible hole trapping occurs no faster than 10 ns. Assuming similar surface passivation between the Fc-hex-SH and Oct-SH exchanged rods and thus a similar distribution of trap states, it is clear that the 10 ns irreversible trapping could not contribute to the 400 ps time constant associated with hole transfer to Fc.

Although the above experimental evidence excludes deep trap mediated charge transfer, there is still the possibility for a two-step charge transfer to Fc via reversible charge transfer to shallow surface trap states. In this case, an equilibrium population of shallow surface trap states could still give rise to photoluminescence. This would not affect the overall PL decay time for the Oct-SH exchanged rods as long as the trap state energy is close to the CdSe HOMO, maintaining an equilibrium between the surface and core states. However, the situation would change in the presence of a Fc hole acceptor especially if the hole rapidly transfers from the shallow trap to the Fc HOMO, thus quenching the PL.

We have shown an example of such a trap state in Figure 7B. This state is associated with the thiolate binding head of the Fc ligand, and its eigenenergy is 0.39 eV below the QD HOMO. Although this trap is significantly lower in its eigenenergy than an ideal reversible trap candidate, the presence of this state in our model system allows us to directly calculate a rate of trap-mediated charge transfer. Using the same procedure as we described above, we found the coupling constants between the Figure 7A and Figure 7B states and between the Figure 7B and Figure 7C states to be 3 and 9 meV, respectively. Both are much larger than the coupling between A and C (which is 0.04 meV), suggesting that trap-mediated hole transfer could dominate the direct hole transfer pathway. We then used a similar procedure to estimate their reorganization energies and used these values to determine the corresponding system total energies following eq 5. We found that $E_B - E_A \approx 0.27$ eV. We then calculated the charge transfer rates from A to B as $k_1 = 6.2 \times 10^{-3}$ (1/ps) and from B to C as $k_2 = 2.3 \times 10^{-2}$ (1/ps). While both transfer rates are significantly faster than the single step transfer rate, the back transfer rate k_1' from B to A is even

dx.doi.org/10.1021/ja500936n | J. Am. Chem. Soc. 2014, 136, 5121−5131

faster because of it being thermodynamically downhill. The detailed balance formula then gives us $k_1' = k_1 \exp(-(E_A - E_B)/(k_B T)) = 2.7 \times 10^2$ (1/ps). Since this rate is much faster than the B to C rate, we can assume an equilibrium between states A and B, with the relative population of B vs A as $\exp((E_A - E_B)/(k_B T)) = 2.3 \times 10^{-5}$. As a result, the overall transition rate will be $k_2 \exp((E_A - E_B)/(k_B T)) = 5.2 \times 10^{-7}$ (1/ps). This is much smaller than the direct A to C hole transfer rate. However, this small rate is a direct consequence of the large $E_B - E_A$ energy difference ($\sim 11 k_B T$), which maintains a very small hole population in the surface trap state. If shallow trap states existed with coupling constants similar to the one studied above but at energies closer to the QD HOMO, then the equilibrium trap population could be orders of magnitude higher resulting in a faster trap-mediated rate compared to the single step transfer. For example, if the $E_A - E_B$ energy difference is less than $8 k_B T$, then the B mediated channel will become faster than the A to C direct transfer. This is assuming that every ligand will have one such intermediate state (e.g., as a result of ideal passivation). If we assume there is only one intermediate trap state for a given QD (e.g., a surface defect state), then this total energy difference must be less than $2 k_B T$ in order for the channel to be competitive with the direct A to C hole transfer. This leaves a rather small energy window ($E_B - E_A < 50$ meV) (since the E_B cannot be smaller than E_A, as precluded by Figure 11) for the existence of such defect states in order to interpret the experimentally observed transition rate as the result of a defect state mediated transition. Whether the charge transfer is trap mediated or coherent therefore depends on the density of surface trap states with energies near the QD HOMO, e.g., whether on average there is a defect surface state within a 50 meV energy window. The PL decays in the Oct-SH exchanged dots indicate a low density of irreversible traps with eigenenergies higher than the QD HOMO state. However, this does not preclude the possibility of a higher density of shallow traps that could play a prominent role in charge transfer, although the chance might not seem high (given the fact the calculated direct A to C transfer rate does agree with the experimentally measured PL decay rate). Further studies will be necessary to settle this issue more firmly.

The rate-limiting hole transfer to the Fc, whether from the QD core or from a shallow surface state, will still have a driving force near 800 meV, which is greater than the calculated reorganization energy, indicating that charge transfer would still be in the inverted region for both cases. This conclusion rests on the assumption that the reorganization energies will not be significantly increased with a localized surface state donor.

CONCLUSION

We have studied the mechanism and rate of hole transfer from a photoexcited CdSe/CdS core/shell nanorod to a tethered ferrocene molecule. Both ab initio calculations and electrochemical measurements were used to determine the driving force (energy alignment) for hole transfer. The good agreement between theory and experiment for this driving force validates the theoretical approach, which adds multiple high level corrections on top of the density functional theory results, including short-range GW correction, polarization correction, and reorganization energies. It also shows that it is possible to use the charge-patching scheme to calculate the electronic structure of a large nanosystem. The rate of hole transfer was measured experimentally with time-resolved PL spectroscopy and corresponded well to calculations based on Marcus theory. The good agreement between the theory and experiment suggests that hole transfer occurs in a single coherent step and is in the Marcus inverted region. However, this model does not consider the presence of surface intermediate states. We calculated the charge transfer rates associated with one of these trap states and found that the coupling constants between this state and both the Fc HOMO and QD HOMO states are significantly larger than the coupling for a direct transfer. Experimental evidence precludes any significant contribution from an irreversible deep trap. However, if there is a significant population of surface states with energies near the QD HOMO, then they could contribute significantly to the QD to Fc charge transfer. Our theoretical surface pseudo-hydrogen passivation model, by design, cannot describe such shallow surface states, although the good agreement between the calculated and experimentally measured charge transfer rate indicates that the role of such possible shallow intermediate states is likely to be small. In either coherent or surface state mediated charge transfer cases, the rate-limiting step will still reside in the Marcus inverted region. These results, therefore, suggest that the charge transfer rate constant can be increased while simultaneously reducing the energetic losses associated with efficient hole extraction. This could be used to design surface-modified QD based solar devices that maximize energy conversion efficiency.

ASSOCIATED CONTENT

Supporting Information

Experimental details for synthesis and measurements. This material is available free of charge via the Internet at http://pubs.acs.org.

AUTHOR INFORMATION

Corresponding Author

lwwang@lbl.gov

Notes

The authors declare no competing financial interest.

ACKNOWLEDGMENTS

The theoretical work (K.T., L.-W.W.) was supported through the Condensed Matter Theory program at Lawrence Berkeley National Laboratory by the Director, Office of Science (SC), Basic Energy Science (BES)/Materials Science and Engineering Division (MSED) of the U.S. Department of Energy (DOE) under Contract DE-AC02-05CH11231. It used resources of the National Energy Research Scientific Computing Center (NERSC) and Oak Ridge Leadership Computing Facility (OLCF) that are supported by the Office of Science of the U.S. Department of Energy, with the computational time allocated by the Innovative and Novel Computational Impact on Theory and Experiment (INCITE) project. The experimental work was supported by the Physical Chemistry of Inorganic Nanostructures Program, KC3103, Director, Office of Science, Office of Basic Energy Sciences of the United States Department of Energy under Contract DE-AC02-05CH11232. Y.S. acknowledges the Miller Institute for Basic Research in Science for a postdoctoral fellowship. J.H.O acknowledges support from a National Science Foundation Graduate Research Fellowship under Grant DGE 1106400.

REFERENCES

(1) Boulesbaa, A.; Issac, A.; Stockwell, D.; Huang, Z.; Huang, J.; Guo, J.; Lian, T. *J. Am. Chem. Soc.* **2007**, *129*, 15132−15133.
(2) Gaponik, N.; Hickey, S. G.; Dorfs, D.; Rogach, A. L.; Eychmuller, A. *Small* **2010**, *6*, 1364−1378.
(3) Bae, W. K.; Kwak, J.; Lim, J.; Lee, D.; Nam, M. K.; Char, K.; Lee, C.; Lee, S. *Nano Lett.* **2010**, *10*, 2368−2373.
(4) Panzer, M. J.; Aidala, K. E.; Anikeeva, P. O.; Halpert, J. E.; Bawendi, M. G.; Bulovic, V. *Nano Lett.* **2010**, *10*, 2421−2426.
(5) Luther, J. M.; Gao, J.; Lloyd, M. T.; Semonin, O. E.; Beard, M. C.; Nozik, A. J. *Adv. Mater.* **2010**, *22*, 3704−3707.
(6) Jang, E.; Jun, S.; Jang, H.; Lim, J.; Kim, B.; Kim, Y. *Adv. Mater.* **2010**, *22*, 3076−3080.
(7) Han, Z.; Qiu, F.; Eisenberg, R.; Holland, P. L.; Krauss, T. D. *Science* **2012**, *338*, 1321−1324.
(8) Wilker, M. B.; Schnitzenbaumer, K. J.; Dukovic, G. *Isr. J. Chem.* **2012**, *52*, 1002−1015.
(9) Amirav, L.; Alivisatos, A. P. *J. Phys. Chem. Lett.* **2010**, *1*, 1051−1054.
(10) Zhu, H.; Song, N.; Lv, H.; Hill, C. L.; Lian, T. *J. Am. Chem. Soc.* **2012**, *134*, 11701−11708.
(11) Kamat, P. V. *Acc. Chem. Res.* **2012**, *45*, 1906−1915.
(12) Shen, Q.; Kobayashi, J.; Diguna, L. J.; Toyoda, T. *J. Appl. Phys.* **2008**, *103*, 084304.
(13) Chakrapani, V.; Baker, D.; Kamat, P. V. *J. Am. Chem. Soc.* **2011**, *133*, 9607−9615.
(14) Robel, I.; Subramanian, V.; Kuno, M.; Kamat, P. V. *J. Am. Chem. Soc.* **2006**, *128*, 2385−2393.
(15) Mora-Ser, I.; Gimnez, S.; Fabregat-Santiago, F.; Gmez, R.; Shen, Q.; Toyoda, T.; Bisquert, J. *Acc. Chem. Res.* **2009**, *42*, 1848−1857.
(16) Marcus, R. A. *J. Chem. Phys.* **1956**, *24*, 966−978.
(17) Marcus, R. A. *Annu. Rev. Phys. Chem.* **1964**, *15*, 155−196.
(18) Robel, I.; Kuno, M.; Kamat, P. V. *J. Am. Chem. Soc.* **2007**, *129*, 4136−4137.
(19) Huang, J.; Huang, Z.; Jin, S.; Lian, T. *J. Phys. Chem. C* **2008**, *112*, 19734−19738.
(20) Sykora, M.; Petruska, M. A.; Alstrum-Acevedo, J.; Bezel, I.; Meyer, T. J.; Klimov, V. I. *J. Am. Chem. Soc.* **2006**, *128*, 9984−9985.
(21) Sharma, S. N.; Pillai, Z. S.; Kamat, P. V. *J. Phys. Chem. B* **2003**, *107*, 10088−10093.
(22) Malicki, M.; Knowles, K. E.; Weiss, E. A. *Chem. Commun.* **2013**, *49*, 4400−4402.
(23) Dorokhin, D.; Tomczak, N.; Velders, A. H.; Reinhoudt, D. N.; Vancso, G. J. *J. Phys. Chem. C* **2009**, *113*, 18676−18680.
(24) Dorokhin, D.; Tomczak, N.; Reinhoudt, D. N.; Velders, A. H.; Vancso, G. J. *Nanotechnology* **2010**, *21*, 285703.
(25) Cyr, P. W.; Tzolov, M.; Hines, M. A.; Manners, I.; Sargent, E. H.; Scholes, G. D. *J. Mater. Chem.* **2003**, *13*, 2213−2219.
(26) Brédas, J. L.; Beljonne, D.; Coropceanu, V.; Cornil, J. *Chem. Rev.* **2004**, *104*, 4971−5004.
(27) Knowles, K. E.; Peterson, M. D.; McPhail, M. R.; Weiss, E. A. *J. Phys. Chem. C* **2013**, *117*, 10229−10243.
(28) Wang, L. W. *Phys. Rev. B* **2002**, *65*, 153410.
(29) Schlamp, M. C.; Peng, X.; Alivisatos, A. P. *J. Appl. Phys.* **1997**, *82*, 5837−5842.
(30) Bruchez, M., Jr.; Moronne, M.; Gin, P.; Weiss, S.; Alivisatos, P. A. *Science* **1998**, *281*, 2013−2016.
(31) Chan, W. C. W.; Nie, S. M. *Science* **1998**, *281*, 2016.
(32) Coe, S.; Woo, W. K.; Bawendi, M.; Bulović, V. *Nature* **2002**, *420*, 800−803.
(33) Pal, B. N.; Ghosh, Y.; Brovelli, S.; Laocharoensuk, R.; Klimov, V. I.; Hollingsworth, J. A.; Htoon, H. *Nano Lett.* **2012**, *12*, 331−336.
(34) Nan, W.; Niu, Y.; Qin, H.; Cui, F.; Yang, Y.; Lai, R.; Lin, W.; Peng, X. *J. Am. Chem. Soc.* **2012**, *134*, 19685−19693.
(35) Carbone, L.; Nobile, C.; Giorgi, M. D.; Sala, F. D.; Morello, G.; Pompa, P.; Hytch, M.; Snoeck, E.; Fiore, A.; Franchini, I. R.; Nadasan, M.; Silvestre, A. F.; Chiodo, L.; Kudera, S.; Cingolani, R.; Krahne, R.; Manna, L. *Nano Lett.* **2007**, *7*, 2942−2950.
(36) Yu, W. W.; Qu, L.; Guo, W.; Peng, X. *Chem. Mater.* **2003**, *15*, 2854−2860.
(37) Noviandri, I.; Brown, K. N.; Fleming, D. S.; Gulyas, P. T.; Lay, P. A.; Masters, A. F.; Phillips, L. *J. Phys. Chem. B* **1999**, *103*, 6713−6722.
(38) Dag, S.; Wang, L. W. *Nano Lett.* **2008**, *8*, 4185−4190.
(39) Wang, L. W. *Annu. Rev. Phys. Chem.* **2010**, *61*, 19.
(40) Wang, L. W. PEtot's Homepage. http://cmsn.lbl.gov/html/PEtot/PEtot.html.
(41) Chu, I. H.; Radulaski, M.; Vukmirovic, N.; Cheng, H. P.; Wang, L. W. *J. Phys. Chem. C* **2011**, *115*, 21409−21415.
(42) Kleinman, L.; Bylander, D. M. *Phys. Rev. Lett.* **1982**, *48*, 1425−1428.
(43) Wang, L. W. *Phys. Rev. B* **1994**, *49*, 10154−10158.
(44) Wang, L. W.; Zunger, A. *J. Chem. Phys.* **1993**, *100*, 2394.
(45) Owen, J. S.; Park, J.; Trudeau, P. E.; Alivisatos, A. P. *J. Am. Chem. Soc.* **2008**, *130*, 12279−12281.
(46) Gomes, R.; Hassinen, A.; Szczygiel, A.; Zhao, Q.; Vantomme, A.; Martins, J. C.; Hens, Z. *J. Phys. Chem. Lett.* **2011**, *2*, 145−152.
(47) Wuister, S. F.; de Mello Donegá, C.; Meijerink, A. *J. Phys. Chem. B* **2004**, *108*, 17393−17397.
(48) Hens, Z.; Martins, J. C. *Chem. Mater.* **2013**, *25*, 1211−1221.
(49) Dowben, P. A.; Waldfried, C.; Komesu, T.; Welipitiya, D.; McAvoy, T.; Vescovo, E. *Chem. Phys. Lett.* **1998**, *283*, 44−50.
(50) Lin, J. -L.; Petrovykh, D. Y.; Kirakosian, A.; Rauscher, H.; Himpsel, F. J.; Dowben, P. A. *Appl. Phys. Lett.* **2001**, *78*, 829−831.
(51) Hedin, L. *Phys. Rev.* **1965**, *139*, A796−A823.
(52) Hybertsen, M. S.; Louie, S. G. *Phys. Rev. B* **1986**, *34*, 5390−5413.
(53) Wang, L. W. *J. Phys. Chem. B* **2005**, *109*, 23330−23335.
(54) Neaton, J. B.; Hybertsen, M. S.; Louie, S. G. *Phys. Rev. Lett.* **2006**, *97*, 216405−216408.
(55) Orlowski, G.; Chawdhury, S.; Kratz, H.-B. *Langmuir* **2007**, *23*, 12765−12770.
(56) Yang, Y.; Yu, L. *Phys. Chem. Chem. Phys.* **2013**, *15*, 2669−2683.
(57) Stranks, D. R. *Discuss. Faraday Soc.* **1960**, *29*, 73.
(58) Krishtalik, L. I.; Alpatova, N. M.; Ovsyannikova, E. V. *Electrochim. Acta* **1991**, *36*, 435−445.
(59) Weber, K. S.; Creager, S. E. *J. Electroanal. Chem.* **1998**, *458*, 17−22.
(60) Lagnnas, M. C.; Pitner, W. R.; Seddan, K. R.; van den Berg, J. *Proc. Electrochem. Soc.* **2003**, *12*, 149−152.
(61) Marcus, R. A. *Rev. Mod. Phy* **1993**, *65*, 599−610.
(62) Luo, Y.; Wang, L. W. *ACS Nano* **2010**, *4*, 91−98.
(63) Kuno, M.; Fromm, D. P.; Hamann, H. F.; Gallagher, A.; Nesbitt, D. J. *J. Chem. Phys.* **2000**, *112*, 3117−3120.
(64) Ip, A. H.; Thon, S. M.; Hoogland, S.; Voznyy, O.; Zhitomirsky, D.; Debnath, R.; Levina, L.; Rollny, L. R.; Carey, G. H.; Fischer, A.; Kemp, K. W.; Kramer, I. J.; Ning, Z.; Labelle, A. J.; Chou, K. W.; Amassian, A.; Sargent, E. H. *Nat. Nanotechnol.* **2012**, *7*, 577−582.
(65) Jones, M.; Lo, S. S.; Scholes, G. D. *Proc. Natl. Acad. Sci. U.S.A.* **2009**, *106*, 3011−3016.